

Article

Investigation of High-Speed Rubbing Behavior of GH4169 Superalloy with SiC/SiC Composites

Zhaoguo Mi ^{1,*} , Kanghe Jiang ², Yicheng Yang ¹, Zhenhua Cheng ², Weihua Yang ^{1,*} and Zhigang Sun ³

¹ College of Energy and Power Engineering, Nanjing University of Aeronautics and Astronauts, Nanjing 210016, China; yangyicheng2013@163.com

² AECC Hunan Aviation Powerplant Research Institute, Zhuzhou 412002, China; peamy@126.com (K.J.); dreamingczh@163.com (Z.C.)

³ Beijing General Research Institute of Mining and Metallurgy, Beijing 100070, China; sun_jg@bgrimm.com

* Correspondence: mizhaoguo@nuaa.edu.cn (Z.M.); yangwh@nuaa.edu.cn (W.Y.)

Abstract: The silicon carbide fiber-reinforced silicon carbide matrix (SiC/SiC), ceramic matrix composite (CMC) and nickel-based superalloy GH4169 can be utilized in high-temperature applications due to their high-temperature performance. The SiC/SiC composites are commonly used in turbine outer rings, where they encounter friction and wear against the turbine blades. This high-speed rubbing occurs frequently in aircraft engines and steam turbines. To investigate the tribological behavior of these materials, rubbing experiments were conducted between the SiC/SiC and the GH4169 superalloy. The experiments involved varying the blade tip speeds ranging from 100 m/s to 350 m/s and incursion rates from 5 $\mu\text{m/s}$ to 50 $\mu\text{m/s}$ at room temperature. Additionally, experiments were conducted at high temperatures to compare the tribological behavior under ambient conditions. The results indicated that the GH4169 superalloy exhibited abrasive furrow wear during rubbing at both room temperature and high temperature. Furthermore, at elevated temperatures, some of the GH4169 superalloy adhered to the surface of the SiC/SiC. The analysis of the experiments conducted at ambient temperatures revealed that the friction coefficient increased with higher blade tip velocities (100–350 m/s). However, the coefficient was lower at high temperatures compared to room temperature. Furthermore, significant temperature increases were observed during rubbing at room temperature, whereas minimal temperature changes were detected on the rubbing surface at high temperatures.

Keywords: SiC/SiC CMCs; nickel-based superalloys GH4169; high-speed rubbing; rubbing mechanism; THE coefficient of friction



Citation: Mi, Z.; Jiang, K.; Yang, Y.;

Cheng, Z.; Yang, W.; Sun, Z.

Investigation of High-Speed Rubbing Behavior of GH4169 Superalloy with SiC/SiC Composites. *Aerospace* **2024**, *11*, 397. <https://doi.org/10.3390/aerospace11050397>

Academic Editor: Spiros Pantelakis

Received: 17 March 2024

Revised: 10 May 2024

Accepted: 13 May 2024

Published: 15 May 2024



Copyright: © 2024 by the authors. Licensee MDPI, Basel, Switzerland. This article is an open access article distributed under the terms and conditions of the Creative Commons Attribution (CC BY) license (<https://creativecommons.org/licenses/by/4.0/>).

1. Introduction

The silicon carbide fiber-reinforced silicon carbide matrix (SiC/SiC) has been selected as an appropriate material for high-temperature components due to its excellent mechanical properties in high-temperature environments. The SiC/SiC has also been identified as a key ceramic matrix composite (CMC) category for aerospace applications and is increasingly being used in hot-end components of aircraft engines. The potential applications of the SiC/SiC include burner liners, blades, and turbine outer rings [1–3]. Nickel-based high-temperature alloys have excellent comprehensive properties in terms of their high-temperature strength, acid and alkali corrosion resistance, wear resistance, and fatigue resistance. Therefore, these alloys are widely used in aviation engines, among which the GH4169 superalloy has the most extensive application range, such as in use in turbine discs, blades, and combustion chambers in aviation engines [4].

The turbines within aircraft engines are critical hot-end components, and the radial clearance between the turbine outer ring and turbine blades seriously affects the effectiveness and reliability of aircraft engines. Instances where rotating components come into contact with stationary ones due to spindle vibration, deformation, or installation

errors can lead to detrimental effects on both the blades and outer rings [5]. When turbine blades rub with the outer ring during operation, they undergo an interaction that generates impact forces on the contact surfaces and frictional forces due to relative motion. These rubbing incidents can lead to wear on either the blades or outer rings. Then, the wearing results in an increase in clearance between the turbine components and a decrease in overall turbine efficiency. Moreover, rubbing occurrences between the blade tips and outer ring may lead to high blade vibratory levels and endanger their structural integrity through fatigue mechanisms [6]. In addition, the impacts of foreign objects on components made of CMCs can result in localized damage and performance degradation over time. This damage can ultimately culminate in catastrophic failures, posing significant risks to turbine functionality and safety. Hence, the phenomenon of blade–outer ring rubbing within turbines exists as a critical issue for ensuring the optimal efficiency and safety in aerospace propulsion systems.

Abradable seal coatings have been widely used in aero-engines to reduce gas path clearance [7–9]. In rotating components, friction pairs are formed when the rotor and stator rub, and the friction damage characteristics of these pairs, formed between different materials, can vary. Over the last decade, several researchers have devoted their attention to investigating friction and wear phenomena across various materials under diverse operating conditions. Their studies have revealed that the friction and wear behavior of composites are influenced by several parameters, including normal load, sliding speed, surface roughness, and lubrication [10–12]. Among these parameters, it has been identified that normal load and sliding velocity are the most influential factors governing the tribological properties of materials [13]. The coefficient of friction of composites sliding against themselves exhibits variable trends depending on the range of operating conditions and the specific sliding pairs selected.

Furthermore, experimental tests conducted by various researchers have focused on investigating the friction and damage characteristics of materials during rubbing processes. At present, high-speed rotating blades are commonly employed to rub both flat [14,15] and curved specimens [16,17] to analyze the friction and wear behavior of the materials forming friction pairs. Some scholars have conducted rubbing experiments using full-ring rubbing [18–20] to understand the frictional mechanical characteristics during the rubbing process; however, the fabrication of the SiC/SiC full rings was difficult.

Few researchers have investigated the rubbing of the SiC/SiC and GH4169. Zhang Na [21] investigated the high-speed rubbing behavior between a Hastelloy-X honeycomb material and a GH4169 superalloy double-stepped labyrinth using a high-speed abrasion test rig. Thermal ablation and oxidation were the main damage occurring on the labyrinth tip and appeared more obviously at a higher blade tip speed. Mengqiu Guo [22] used a high-temperature and high-speed rubbing experimental platform to test the rubbing damage of the SiC/SiC flat and DD6 metal at 1100 °C. The results showed that the DD6 metal became significantly worn. In the experiment, although the friction coefficient of the specimen during rubbing was measured, due to the use of flame heating, the flame interfered with the measurement of force. Additionally, the use of blades and flat plates for rubbing rendered the friction coefficient obtained during the process inaccurate. The experimental studies on the damage characteristics of materials during rubbing processes often employ high-speed rotating tables to drive the blades for testing. Further research is needed on the impact of wear damage and friction characteristics on the SiC/SiC composite and GH4169 superalloy materials.

The purpose of this paper was to investigate the friction and wear properties of friction pairs composed of the GH4169 superalloy and SiC/SiC manufactured by MI technology at high speeds. The experiment utilized a high-speed rig to research the wear mechanisms of SiC/SiC and GH4169. The tests were conducted at a fixed contact azimuth angle to examine the friction coefficient at various rubbing speeds and to observe the friction and wear behavior. Additionally, experiments were performed on the high-speed rubbing of the SiC/SiC and GH4169 superalloy at 1000 °C. The findings of this study will contribute

to the analysis of wear and frictional faults between the GH4169 superalloy and SiC/SiC in both dynamic and static contact components, offering insights for processing the GH4169 superalloy using SiC/SiC CMCs.

2. Materials and Methods

2.1. Materials

The blade sample used for the rub test was made of GH4169 superalloy, commonly employed in compressor blade production. The blade sample was flat, with the rubbed face measuring $13 \text{ mm} \times 0.5 \text{ mm}$ square. The SiC/SiC samples were fabricated using the melt infiltration (MI) method, forming 30° circular arc-shaped thin sheets with a radius of 164 mm, a thickness of 3.75 mm, and a width of 28 mm. These samples featured a cross-ply fiber architecture $[0^\circ/90^\circ/90^\circ/0^\circ]$, with the volume fraction of SiC fibers in the SiC matrix set at 24%. The average diameter of the fibers was $10.9 \mu\text{m}$, and the average interface layer thickness was $0.3 \mu\text{m}$. The interface layer, crucial for connecting the fiber and matrix, significantly influences the composite's properties. Pyrolytic carbon (PyC) and hexagonal boron nitride (h-BN) are recognized as effective interface layers for SiC/SiC composites due to their layered microstructure. However, the PyC interface layer is prone to oxidation in oxidizing atmospheres, even at lower temperatures, leading to the degradation of mechanical properties. Conversely, the BN interface layer enhances the oxidation resistance of SiC/SiC composites. A thin boron nitride (BN) interphase was deposited on the surfaces of the SiC fibers using the chemical vapor infiltration (CVI) process. The samples are illustrated in Figure 1.

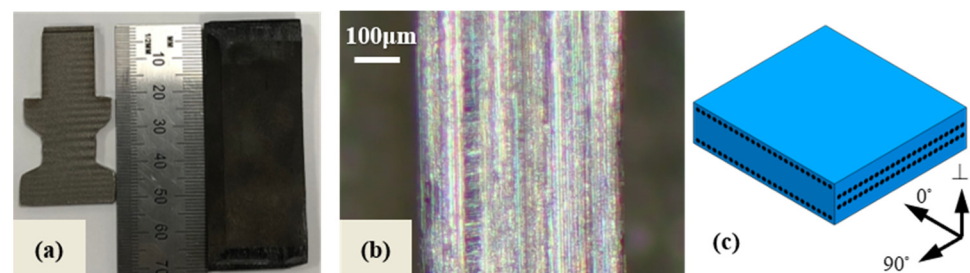


Figure 1. The SiC/SiC sample and blade: (a) the blade and the sample; (b) the morphology of the blade tip; (c) the schematic of the SiC/SiC composites.

The design of the GH4169 superalloy blade prioritizes ease of processing and installation. To maintain a constant force during the rubbing, it is crucial to minimize the contact surface between the GH4169 superalloy and the SiC/SiC while ensuring a fixed rubbing position. The root of the blade was a special external structure designed to be installed on the wheel disc. The blade design had a fixture, and the blade fixture was connected to the turntable using a tree-shaped tenon groove. In addition, to ensure the rubbing requirements, sharp protrusions were designed at both ends of the SiC/SiC. Before rubbing, the surface of the GH4169 superalloy blade tip had uniform scratches in the length direction of the blades due to machining.

2.2. The Rig

The rubbing tests were performed on a high-speed rubbing rig (BKVHVT 300/800; Beijing General Research Institute of Mining and Metallurgy, Beijing, China). A schematic of the test rig is shown in Figures 2 and 3. The rubbing rig could reach a maximum linear speed of 502 m/s using a rotary 640 mm diameter disk with a maximum rotational speed of 15,000 rpm. A blade sample was installed on a rotating disk, and a counterweight blade shorter than the sample was fixed on the disk at 180° to balance its centrifugal force. The diameter of the flat blade tip was 681 mm. During the rubbing test, a high-speed flame was generated from the heat module, which could cover and heat the sample surface.

The SiC/SiC was a thin, circular arc sheet with sharp corners, fixed on a micro-motion two-dimensional displacement platform using a customized fixture.

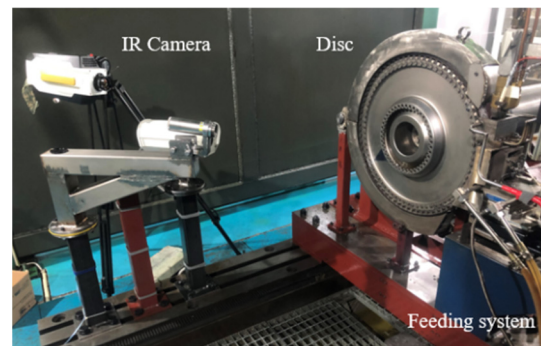


Figure 2. The measurement of temperature and force.

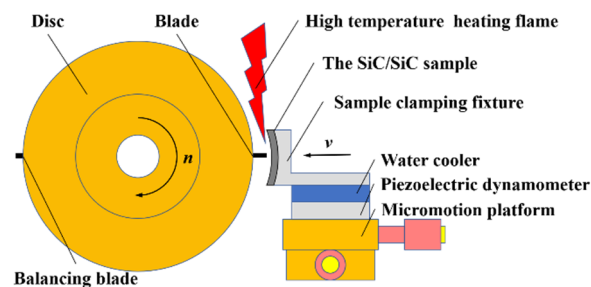


Figure 3. A schematic diagram of the test rig.

The speed range of the displacement platform was 2–2000 $\mu\text{m}/\text{s}$. A three-dimensional force measurement platform was arranged on the micromotion platform, and a three-component piezoelectric dynamometer with a maximum measurement force of 5000 N and a 500 g accelerometer was used to measure the rubbing force and dynamic impact response between the GH4169 superalloy and the SiC/SiC tips during the rubbing test process. The Kistler 9257B multi-component dynamometer (Kistler Group, Winterthur, Switzerland) was selected to measure the radial and tangential friction forces, as shown in Figure 2, and a PCB 352C41 micro piezoelectric accelerometer (PCB Piezoelectric, Beijing, China) was installed with a measurement range of ± 500 g on the board to measure the dynamic impact response during the friction process. A high-speed data acquisition system, GEN3i, with a GN815 data acquisition card was used to record these signals at a sampling frequency of 100 kHz per channel. The temperature during the test was measured using an IR (infrared thermal) camera (Telops Inc., Quebec, QC, Canada), and the highest measurement frequency of temperature was 2500 Hz. The IR camera measures temperatures within the range of 0–1500 $^{\circ}\text{C}$ and records the temperature changes.

2.3. Testing Scheme

The wear behavior between the GH4169 superalloy and the SiC/SiC is influenced by various factors, such as rubbing speed, intrusion rate, and temperature. In this study, a test matrix was designed to investigate the effects of friction velocity and intrusion velocity on the friction of the GH4169 superalloy and the SiC/SiC. This test matrix was also used in the study of the influences of blade tip speed and incursion rate of the type which may be encountered in aero-engines, and ten rubbing test parameters are shown in Table 1. In this series of tests, the blade tip velocity varied between 100 and 150 m/s and the incursion rate varied between 5 and 50 $\mu\text{m}/\text{s}$ under ambient temperatures. The high-temperature rubbing test was performed, with a blade tip velocity of 100 m/s and an incursion rate of 5 $\mu\text{m}/\text{s}$. During the rubbing process, the blades were constantly worn, so the depth of each

rubbing was only related to the blade's linear speed and feed rate. The incursion depth per pass was considered in the rubbing test. During the friction process, the blade rubbed against the SiC/SiC every time it rotated, and the contact surface of each rubbing was the blade's cross-section. Therefore, each rubbing during the rubbing process was identical, regardless of the depth of rubbing.

Table 1. The test parameters used in this work.

Test No.	Blade Tip Velocity, u (m/s)	Incursion Rate, v ($\mu\text{m/s}$)	Incursion Depth per Pass (μm)	Temperature
1#	100	5	0.11	Ambient temperature
2#	100	10	0.21	Ambient temperature
3#	100	20	1.07	Ambient temperature
4#	225	5	0.05	Ambient temperature
5#	225	10	0.10	Ambient temperature
6#	225	50	0.48	Ambient temperature
7#	350	5	0.03	Ambient temperature
8#	350	10	0.06	Ambient temperature
9#	350	50	0.31	Ambient temperature
10#	100	5	0.11	900~1100 °C

In the test, when the turntable was driven by the motor, the blade tip speed increased until the target speed was reached. Then, the feed platform drove the SiC/SiC sample to ensure that the feed platform moved at a fixed speed. When a collision occurred, the feed platform received a trigger signal to start recording the feed depth until it reached the set feed depth. When the experiment reached the feed stage, the feed platform returned to its initial position.

When the disk's speed reached the target value and was kept stable, the SiC/SiC sample would be driven by the radial feed system to move quickly to the blade until the blade tip came into contact with the sample surface. The SiC/SiC sample was then further fed at the desired incursion rate provided in Table 1 for a period until the total incursion depth was finished. Once the target incursion depth was attained, the platform retreated quickly to the initial position, and then the blade and the SiC/SiC sample were dismantled for further analysis after the disk stopped.

2.4. Measurements

Figure 4 shown the rubbing positions of the blade on the SiC/SiC sample. The vertical distance from the rubbing position to the rotation axis of the dish is denoted as H , with a height of 30 mm. The rotation diameter of the rubbing point is denoted as R , with a length of 651 mm, which is the same as the radial length of the blade tip of the GH4169 superalloy sample. The azimuth angle θ at the rubbing position can be calculated as 0.157 radians using geometric relationships.

The GH4169 superalloy blade rubbing with the SiC/SiC sample was as shown in Figure 5. During a test, the blade incursion depth was fixed at the macro scale. The real incursion was continuously evolving due to the rugosity at the micro-scale. During the friction process, each rotation of the blade resulted in rubbing against the SiC/SiC, with the contact surface being the blade's cross-section. As a result, each rubbing instance during the process remained consistent, irrespective of the depth of rubbing.

The force during rubbing was associated with the azimuth angle; therefore, the direction of the force was constant and transient. The tangential force and radial force in a rubbing can be calculated by F_x and F_z , as shown in the following:

$$\begin{cases} F_{\text{radial}} = F_x \cos \theta - F_z \sin \theta \\ F_{\text{tangential}} = F_x \sin \theta + F_z \cos \theta \end{cases} \quad (1)$$

The coefficient of friction μ can be calculated using the following equation:

$$\mu = \frac{F_{\text{tangential}}}{F_{\text{radial}}} \quad (2)$$

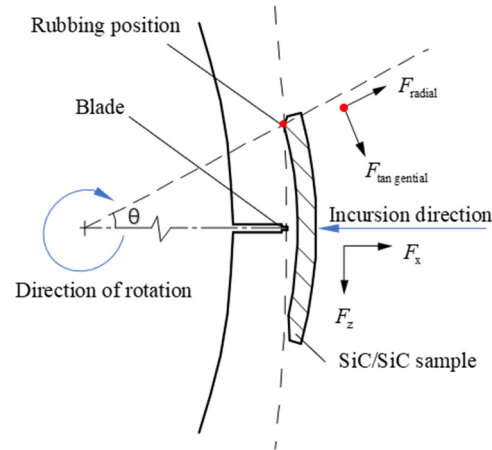


Figure 4. The rubbing positions of the blade on the SiC/SiC sample.

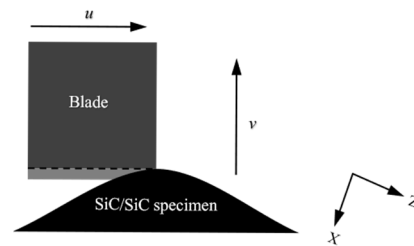


Figure 5. A schematic representation of the incursion.

3. Results and Discussion

3.1. Analysis of Wear Surface Morphology

Two types of wear are described, as follows: (i) a polished appearance, corresponding to the application of a harmonious layer of wear residue, resulting in a nearly flat surface due to this phenomenon; (ii) a rough morphological structure caused by the uneven wear of the composite matrix and low adhesion fibers or powder residues. The first type of residual film has a lubricating effect and reduces contact pressure, thereby reducing the friction and wear coefficients [23]. The morphology of the SiC/SiC sample and GH4169 superalloy blade tip were distinctive at different temperatures. The wear mechanisms mainly included abrasive wear, oxidation wear, and delamination wear at 500 °C. However, the adhesive wear and oxidation wear subsequently became dominant in the wear mechanisms at 700 °C [24].

After the rubbing test, the surface morphology of both the SiC/SiC sample and GH4169 superalloy blade tip, worn under different temperatures, was obtained. Figure 6a shows the surface morphologies after rubbing at an ambient temperature. Black rubbing marks are shown at the rubbing position of the SiC/SiC sample. However, noticeable wear can be observed on the GH4169 superalloy blade tip. Figure 6b shows the surface morphologies after rubbing at temperatures ranging from 900 to 1100 °C. These photos reveal a metal adhesion layer on the rubbing position of the SiC/SiC sample, and wear was also observed on the GH4169 blade tip. While wear occurred in the friction pair of the SiC/SiC sample and GH4169 superalloy at various temperatures, the wear mechanisms differed based on the temperature conditions under which the SiC/SiC sample surface was rubbed. When the SiC/SiC material was at a temperature of 900 °C, the worn GH4169 softened and adhered to the surface of the SiC/SiC material.

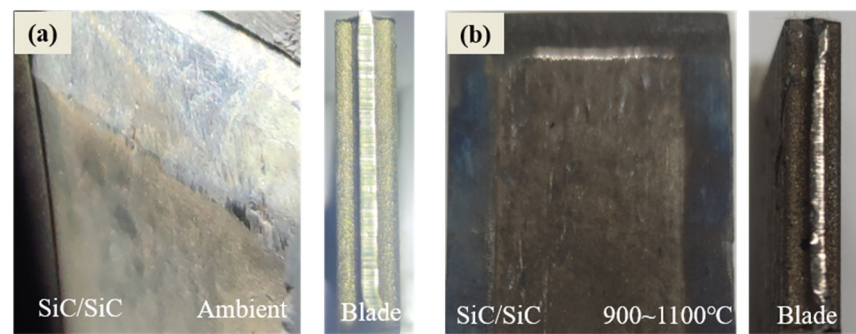


Figure 6. The surface morphologies of the blade tip and the SiC/SiC samples rubbed at (a) ambient temperature and (b) 900~1100 °C.

To elucidate the wear mechanisms, the worn surfaces of blade tip were observed.

In Figure 7a, the wear surface exhibits furrow wear, with irregularities present at the boundary. In Figure 7b, the wear surface and the boundary are worn, but the surface is smoother. Some GH4169 superalloys can soften and stack along the rub direction. In addition, spalling occurred on the wear surface. As can be seen, at the opposite side of the rub direction on the rubbed blade tip, material accumulation was found during the two measurements. The designer, producer, and maintainer of the aero-engines call this phenomenon shear lip or edge curl [15].

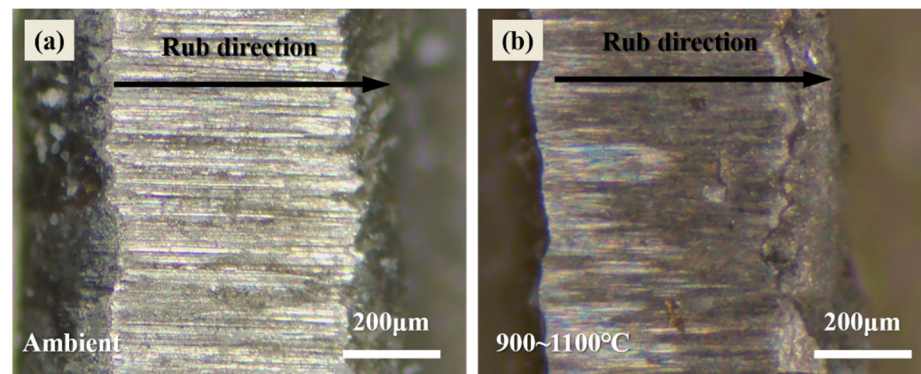


Figure 7. The morphologies of the blade tip wear scars: (a) ambient temperature; (b) between 900 and 1100 °C.

In the initial stages of rubbing, the squeezing effect of the friction pair induced a softening of the GH1469 superalloy blade tip. This softening led to the accumulation of the GH1469 superalloy at the initial position of the blade tip, in the opposite direction of the rubbing. The softening became more pronounced at temperatures ranging from 900 to 1100 °C, resulting in the increased accumulation of the GH1469 superalloy at the starting position of rubbing. As the rubbing process progresses, the GH1469 superalloy then experienced wear. At room temperature, the rough rubbing surface of the SiC/SiC led to furrow wear formation on the blade tip during rubbing. However, when the rubbing occurred at temperatures between 900 and 1100 °C, the blade tip was heated by the SiC/SiC, causing the contacted GH1469 superalloy to soften. Consequently, a portion of the softened GH1469 superalloy adhered to the surface of the SiC/SiC, forming a layer that reduced the roughness of the rubbing surface. Furthermore, the remaining softened GH1469 superalloy slid along the rubbing direction, forming a softening layer on the GH1469 superalloy. This softening layer may detach during rubbing due to its weak adhesion to the blade. The surface wear morphology of the rubbed surface indicates that, in the rubbing between the SiC/SiC and GH1469 superalloy, wear predominantly occurred on the contact surface of the GH1469 superalloy blade tip. At an ambient temperature, the friction behavior was mainly abrasive wear, as evidenced with the wear occurring on the GH1469 superalloy

blade tip. At temperatures ranging from 900 to 1100 °C, the friction behavior shifted to mainly adhesive wear.

3.2. Analysis of Rubbing Test

The rubbing was periodic throughout the test process. With each rotation of the rubbing blade, relative sliding occurred between the surface of the SiC/SiC and the tip of the GH4169 superalloy blade. Any changes in temperature on the surface of the SiC/SiC sample before and after rubbing were monitored using an infrared thermal imager. Before commencing the experiment, the temperature of the SiC/SiC was calibrated using a thermistor to ensure accurate measurements using the infrared thermal imager.

The measurement results of the temperature and force after each rubbing are shown in Figure 8. In the figure, (a)~(d) represent the infrared measurement results of the surface temperature on the SiC/SiC samples at four time points before and after rubbing. In the contact area, there is a temperature increase area after multiple rubbings. It is evident that the temperature change area was localized primarily near the rubbing area. The highest temperature recorded during the rubbing process serves as a reflection of the intensity of frictional heat generation in the specimen. Therefore, the highest temperature observed in the local area was selected as the characteristic temperature T . The changes in T exhibited periodic behavior throughout the duration of the test. The highest temperature remained unchanged per rubbing. The T was 47 °C before rubbing, rapidly rose to 120 °C after the rubbing, and then decreased to 47 °C before the next rubbing. When the rubbing occurred, the force could be measured in both the X and Z direction. The measured forces exhibited attenuated vibrations during the test. It can be seen that the measured force suddenly increased and underwent attenuated vibration, and this attenuation was then eliminated before the next rubbing. When a collision occurred, the blade exerted an instantaneous force on the SiC/SiC sample, and the SiC/SiC sample underwent a damping vibration after excitation. The testing mechanism can be described as a mass–spring–damper system; an attenuation response was generated when the rubbing force is input, and this could be simplified and represented as a rectangular pulse force [21]. Therefore, the force exerted during each rubbing period remained constant and corresponded to the measured maximum force. The force of rubbing was the maximum F_x and F_z components. The temperature change during the rubbing process corresponded to the variation in the rubbing force.

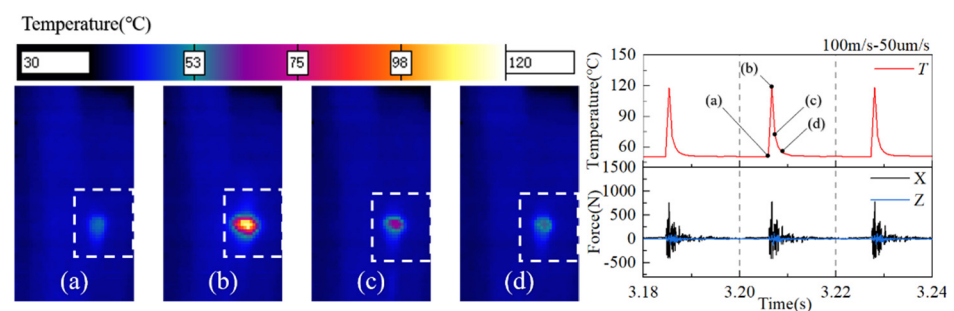


Figure 8. The typical rubbing temperatures and forces over time for the rubbing cycle: (a) before rubbing; (b–d) after rubbing, with the maximum value of T within the specified box area.

The analysis of the measurement results reveals that T reached its peak as rubbing was finished. Following rubbing, a notable temperature increase occurred in the rubbing area. Subsequently, the temperature rapidly decreased until it reached a distribution similar to that before rubbing. The heating flux generated on the contact area of the SiC/SiC sample due to friction can be considered as a form of semi-infinite heat transfer. The heat was primarily conducted inside the SiC/SiC sample through thermal conduction. When the blade disengaged from the SiC/SiC sample, the convective heat transfer on the SiC/SiC sample was significantly intensified, leading to a swift decrease in temperature.

3.3. Force Analysis

Based on the analysis above, the maximum value of the force in each rubbing was taken as the horizontal force F_x and vertical force F_z . For each rubbing, the maximum T and the minimal T represent the temperature T_{Rubbing} and T_0 of the SiC/SiC samples before and after rubbing, respectively.

Figure 9 shows the rubbing force and the temperature under ambient conditions. Taking the blade tip velocity of 100 m/s and incursion rate of 10 $\mu\text{m/s}$ as an example, during the test process, in the initial stage of the test (0.45 s~7.2 s), the F_x and F_z first increased significantly and then slowly increased. At the same time, the heat generated by each rubbing also increased. In the middle stage of the test process (7.2 s~11.7 s), with the increased rubbing feed stroke, the variation in F_x and F_z tended to stabilize, and the corresponding rubbing temperature also tended to stabilize. At the end stage of rubbing (11.7 s~11.8 s), the F_x and F_z rapidly decreased to 0.

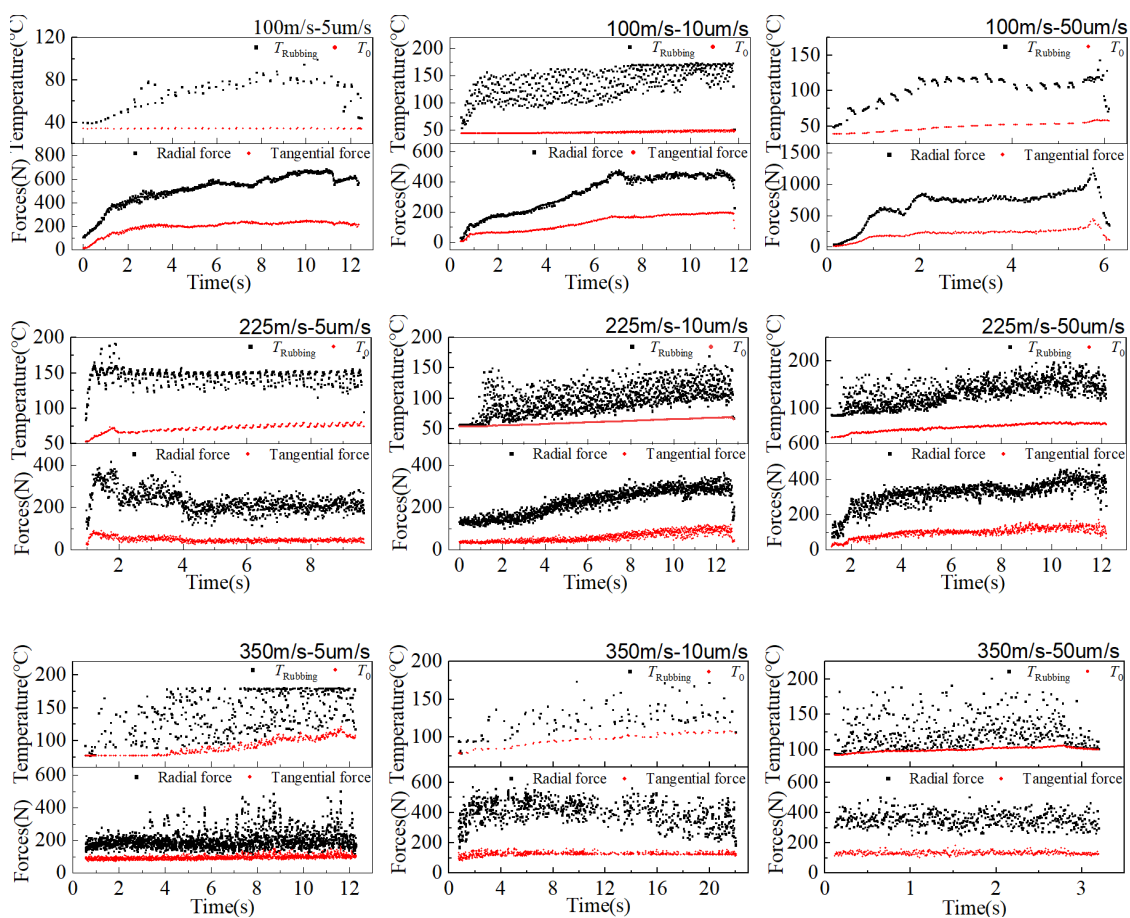


Figure 9. The rubbing forces and temperature under ambient conditions.

Each test process consisted of three stages: the pre-rubbing stage, the rubbing stage, and the termination stage. The pre-rubbing stage refers to the stage where the contact area between the blade tip and the SiC/SiC sample was not stable; however, the blade tip velocity and the incursion rate remained unchanged. As the rubbing deepened, the rubbing area continued to increase. During this stage, the blade tip velocity and the incursion depth of the local rubbing surface were smaller than the other rubbing surfaces. During the test, the rubbing area remained unchanged, while the blade tip velocity and incursion rate also remained unchanged, achieving stable rubbing. During the termination stage, the blade tip velocity and area were unchanged, but the incursion depth gradually reached 0. Therefore, both the force and temperature quickly decreased to the initial state.

3.4. The Coefficient of Friction

When the high-speed rotating blade skimmed across the tip of the SiC/SiC sample, it initiated sliding friction between the blade tip and the SiC/SiC surface. Based on the surface morphology of the sample, it is evident that the GH4169 blade tip experienced frictional wear. The coefficient of friction was determined using Equation (2), and its values are shown in Figure 10. Taking the example of a blade tip velocity of 100 m/s and an incursion rate of 10 $\mu\text{m/s}$, during the period from 0 to 2 s, the coefficient of friction increased from 0.2 to 0.5, and then rapidly decreased to 0.34. During the period from 2 to 11 s, the friction coefficient remained at 0.36. Between 11 and 12 s, the friction coefficient increased to 0.48. This result indicates a rapid increase in the coefficient of friction followed by a decrease during the pre-test stage. The friction coefficient remained unchanged during the test stage; however, it increased significantly during the test termination stage. Initially, the rubbing surface had not yet achieved stability. As the test progressed, the rubbing surface continuously expanded. Simultaneously, the increased rubbing surface altered the roughness, leading to significant changes in the coefficient of friction during the pre-test stage. Throughout the test stage, the rubbing surface remained constant. As stable roughness developed between the test surface and the SiC/SiC sample, the friction coefficient remained unchanged during this phase. In the final stage, while the roughness of the rubbing surface remained stable, the feed rate gradually decreased until no further rubbing occurred. As the incursion depth decreased, there was a slight increase in the coefficient of friction.

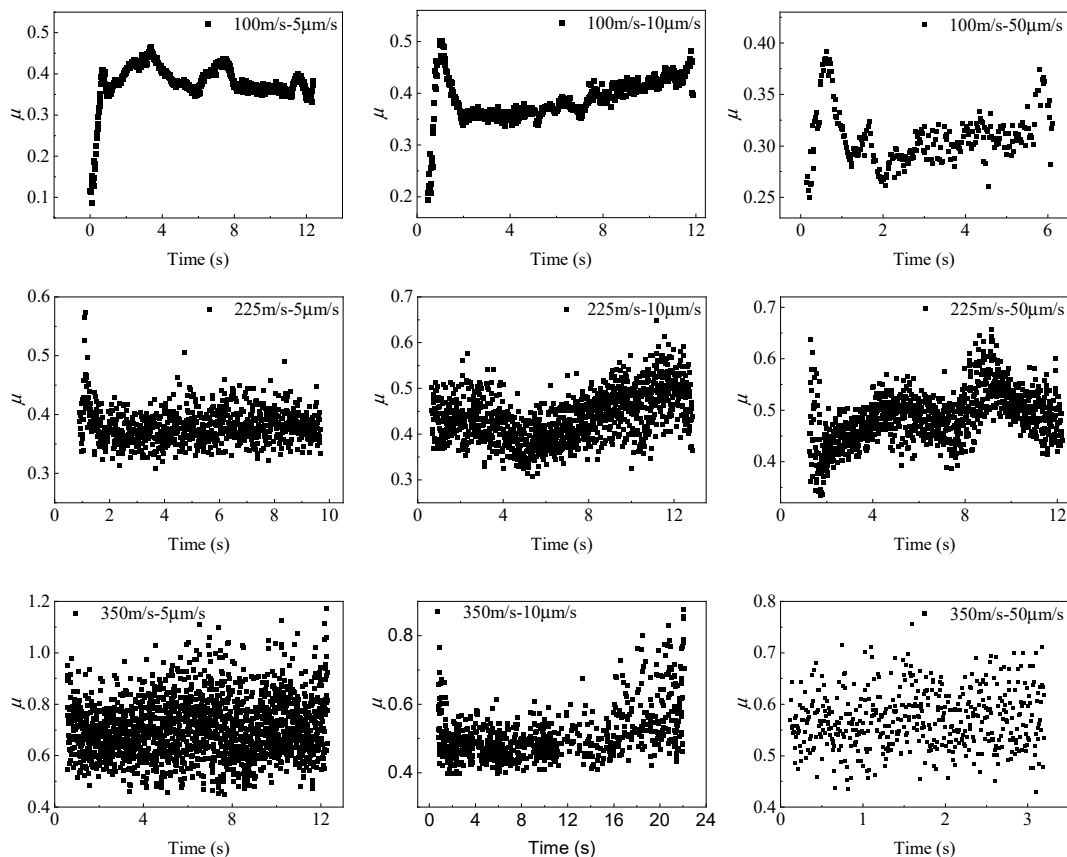


Figure 10. The coefficient of friction under ambient conditions.

3.5. The Rubbing under High Temperatures

Given that the SiC/SiC operates in high-temperature environments, it is crucial to recognize that the rubbing and wear conditions differ significantly compared to those experienced at room temperatures. Before the rubbing process, the SiC/SiC sample was

preheated using a flame heater. Once the surface temperature of the sample reached 1200 °C, heating ceased, and the rubbing process commenced. As shown in Figure 11, the rubbing surface underwent a convective heat exchange with the surrounding environment, leading to a rapid decrease in the surface temperature. The highest temperature on the rubbing surface did not exhibit a significant increase during the rubbing process. Throughout the test process, the force initially increased, then decreased, and eventually stabilized. Once the entire rubbing process reached stability, the force remained constant. Toward the conclusion of the test, the force rapidly decreased to zero.

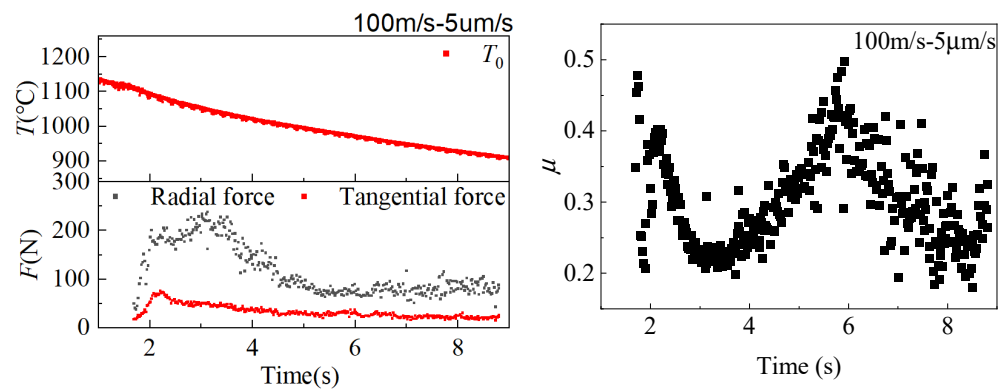


Figure 11. The rubbing forces, temperature, and coefficient of friction at 900~1100 °C.

The friction coefficient serves as a crucial indicator of the force characteristics during rubbing, playing a pivotal role in the analysis of forces during this process. At the onset of the testing process, stability was not attained in the experiment. Hence, the results from the mid-term stage of each test were chosen to obtain statistics for determining the friction coefficient. In Figure 12, the coefficient of friction and temperature are presented. The difference ΔT between T_{Rubbing} and T_0 represents the temperature increase caused by rubbing. It reflects the intensity of heat generated by the friction process. The results indicate that, with a constant blade tip velocity, the intrusion rate had a relatively minor effect on the friction coefficient. However, at a specific intrusion rate, an increase in blade tip velocity corresponded to a higher friction coefficient in the ambient temperature. For an incursion of 5 $\mu\text{m/s}$, the coefficients of friction were 0.36 at 100 m/s, 0.44 at 225 m/s, and 0.70 at 350 m/s. Under these conditions, the cutting mechanism overcame the radial extrusion, smearing, and other mechanisms. As the blade tip speed increased, the cutting action gradually became the predominant failure mode, accompanied by smearing. With a fixed incursion rate and blade tip velocity, the coefficient of friction was higher under ambient temperatures compared to high temperatures (900~1100 °C). The coefficient of friction is measured at 0.31 during the 900~1100 °C temperature range. Under these conditions, the smearing mechanism predominated. Therefore, with the increase in the SiC/SiC sample temperature, the cutting action gradually diminished. The temperature change observed during friction revealed a notable increase in temperature in the SiC/SiC material at ambient temperature. However, once the temperature of the SiC/SiC material reached 900 °C, the temperature increase during the friction process became negligible.

Based on the analysis above, it can be inferred that the velocity at the tip of a turbine blade significantly influences the overall friction coefficient during rubbing. The increase in the friction coefficient indicates an increase in the proportion of friction force during the friction process; consequently, this might lead to an increase in the torque exerted on the blade. Higher radial velocity during the wear process exacerbates the impact of the blade on the outer ring, thus increasing the torque borne by the blade. Consequently, when designing blade strength, it is imperative to consider the friction conditions under high-speed rotation and high radial speed for verification. Additionally, in the collision between the SiC/SiC outer ring and the GH4169 blades, there is no need to account for the

impact of thermal stress resulting from sudden rises in temperature on the SiC/SiC during the collision and wear process of the outer ring.

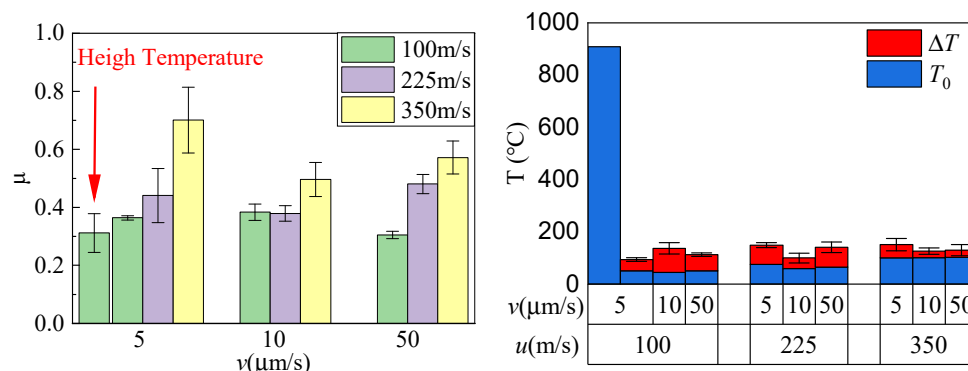


Figure 12. The value of the coefficient of friction and temperature.

4. Conclusions

As a potential material for high-temperature components, SiC/SiC is under consideration for use in turbine outer rings. This study aimed to deepen our understanding of the high-speed rubbing behavior between the SiC/SiC and GH4169 superalloy blades. This investigation delved into the friction and wear characteristics at blade tip velocities ranging from 100 to 350 m/s and incursion rates from 5 to 50 $\mu\text{m/s}$ at an ambient temperature. Furthermore, a comparison can be drawn between the friction and wear behavior during rubbing at an ambient temperature and elevated temperatures of 900~1100 $^{\circ}\text{C}$.

- (1) The GH4169 superalloy material incurred plowing wear on the blade tip, while the SiC/SiC did not show any significant scraping damage on the surface. At high temperatures, the GH4169 superalloy adhered to the SiC/SiC sample rubbing surface. The GH4169 superalloy material exhibited plowing wear on the blade tip, whereas the SiC/SiC did not exhibit significant scraping damage on its surface. At elevated temperatures, the GH4169 superalloy adhered to the SiC/SiC sample's rubbing surface.
- (2) When the incursion rate remained constant, the coefficient of friction rose with increasing blade tip speeds. For instance, at an incursion rate of 5 $\mu\text{m/s}$, the friction coefficients were 0.36 at 100 m/s, 0.44 at 225 m/s, and 0.70 at 350 m/s. Significant temperature increases were observed during rubbing at room temperature, whereas no notable temperature increases occurred on the surface of the SiC/SiC during rubbing at high temperatures.

Author Contributions: All authors contributed to the study's conception and design. Material preparation, data collection, and analysis were performed by Z.M. The first draft of the manuscript was written by Z.M., and all authors commented on previous versions of the manuscript. All authors have read and agreed to the published version of the manuscript.

Funding: This research received no external funding.

Data Availability Statement: Data are contained within the article.

Conflicts of Interest: The authors declare no conflicts of interest.

References

1. Beesley, C.P. The application of CMCs in high integrity gas turbine engines. *KEM* **1996**, *127–131*, 165–176. [[CrossRef](#)]
2. Christin, F. Design, fabrication, and application of thermostructural composites (TSC) like C/C, C/SiC, and SiC/SiC composites. *Adv. Eng. Mater.* **2002**, *4*, 903–912. [[CrossRef](#)]
3. Snead, L.L.; Henager, C.H., Jr.; Nozawa, T.; Hinoki, T.; Iveković, A.; Novak, S.; De Vicente, S.G. Current status and recent research achievements in SiC/SiC composites. *J. Nucl. Mater.* **2014**, *455*, 387–397. [[CrossRef](#)]
4. Pollock, T.M.; Tin, S. Nickel-based superalloys for advanced turbine engines: Chemistry, microstructure and properties. *J. Propul. Power* **2006**, *22*, 361–374. [[CrossRef](#)]

5. Langenbrunner, N.; Weaver, M.; Dunn, M.G.; Padova, C.; Barton, J. Dynamic response of a metal and a CMC turbine blade during a controlled rub event using a segmented shroud. *J. Eng. Gas Turbines Power* **2015**, *137*, 062504. [[CrossRef](#)]
6. Berthoulet, B.; Batailly, A.; Stainier, L.; Legrand, M.; Cartraud, P. Phenomenological modeling of abradable wear in turbomachines. *Mech. Syst. Signal Process.* **2018**, *98*, 770–785. [[CrossRef](#)]
7. Xue, W.; Gao, S.; Duan, D.; Zhang, J.; Liu, Y.; Li, S. Effects of blade material characteristics on the high-speed rubbing behavior between Al-hBN abradable seal coatings and blades. *Wear* **2018**, *410*, 25–33. [[CrossRef](#)]
8. Gao, S.; Xue, W.; Duan, D.; Li, S.; Zheng, H. Effect of thermal–physical properties on the abradability of seal coating under high-speed rubbing condition. *Wear* **2018**, *394–395*, 20–29. [[CrossRef](#)]
9. Liu, Y.D.; Zhang, J.P.; Pei, Z.L.; Liu, J.H.; Li, W.H.; Gong, J.; Sun, C. Investigation on high-speed rubbing behavior between abrasive coatings and Al/hBN abradable seal coatings. *Wear* **2020**, *456–457*, 203389. [[CrossRef](#)]
10. Kumar, A.; Rana, R.S.; Purohit, R.; Namdev, A.; Saxena, K.K.; Kumar, A. Optimization of dry sliding wear behavior of Si₃N₄ and Gr reinforced Al-Zn-Mg-Cu composites using Taguchi method. *J. Mater. Res. Technol.* **2022**, *19*, 4793–4803. [[CrossRef](#)]
11. Sanman, S.; Manjunath, A.; Prashanth, K.; Shadakshari, R.; Sunil, S. An experimental study on two body abrasive wear behavior of natural fiber reinforced hybrid polymer matrix composites using Taguchi analysis. *Mater. Today Proc.* **2022**; *in press*.
12. Gomes, J.; Silva, O.; Silva, C.; Pardini, L.; Silva, R. The effect of sliding speed and temperature on the tribological behaviour of carbon–carbon composites. *Wear* **2001**, *249*, 240–245. [[CrossRef](#)]
13. Ruggiero, A.; Merola, M.; Carlone, P.; Archodoulaki, V.-M. Tribo-mechanical characterization of reinforced epoxy resin under dry and lubricated contact conditions. *Compos. Part B Eng.* **2015**, *79*, 595–603. [[CrossRef](#)]
14. Xue, W.; Gao, S.; Duan, D.; Wang, L.; Liu, Y.; Li, S. Study on the High-Speed Rubbing Wear Behavior Between Ti6Al4V Blade and Nickel–Graphite Abradable Seal Coating. *J. Tribol.* **2017**, *139*, 021604. [[CrossRef](#)]
15. Xue, W.; Gao, S.; Duan, D.; Zheng, H.; Li, S. Investigation and simulation of the shear lip phenomenon observed in a high-speed abradable seal for use in aero-engines. *Wear* **2017**, *386*, 195–203. [[CrossRef](#)]
16. Lu, B.; Ma, X.; Wu, C.; Xuan, H.; Hong, W. The wear of seal fins during high-speed rub between labyrinth seal fins and honeycomb stators at different incursion rates. *Materials* **2021**, *14*, 979. [[CrossRef](#)]
17. Nitschke, S.; Wollmann, T.; Ebert, C.; Behnisch, T.; Langkamp, A.; Lang, T.; Gude, M. An advanced experimental method and test rig concept for investigating the dynamic blade-tip/casing interactions under engine-like mechanical conditions. *Wear* **2019**, *422*, 161–166. [[CrossRef](#)]
18. Munz, O.; Pychynski, T.; Schwitzke, C.; Bauer, H.-J. Continued experimental study on the friction contact between a labyrinth seal fin and a honeycomb stator: Slanted position. *Aerospace* **2018**, *5*, 82. [[CrossRef](#)]
19. Yang, Y.; Chang, J.; Mi, Z.; Yang, W. Experimental and Numerical Study on the Influence of Rubbing Force on Radial Crack Initiation in Labyrinth Seal Fins. *Aerospace* **2022**, *9*, 831. [[CrossRef](#)]
20. Yang, Y.; Mi, Z.; Zhang, W.; Chang, J.; Liu, Y.; Zhong, B.; Yang, W. Experimental Study on the Effect of Rubbing Mode on Radial Crack Initiation in Labyrinth Seal Fins of Shrouded Turbine Blade. *Aerospace* **2022**, *9*, 441. [[CrossRef](#)]
21. Zhang, N.; Shen, J.; Xuan, H.; Hu, Y.; Hong, W. Evaluation of an alsi-polyester abradable seal coating performance using high-temperature and high-velocity abrasion tests. *Proc. Inst. Mech. Eng. Part J J. Eng. Tribol.* **2016**, *230*, 842–851. [[CrossRef](#)]
22. Guo, M.; Cui, Y.; Wang, C.; Jiao, J.; Bi, X.; Tao, C. Design and characterization of BSAS-polyester abradable environmental barrier coatings (A/EBCs) on SiC/SiC composites. *Surf. Coat. Technol.* **2023**, *465*, 129617. [[CrossRef](#)]
23. Birleanu, C.; Pustan, M.; Pop, G.; Cioaza, M.; Popa, F.; Lazarescu, L.; Contiu, G. Experimental Investigation of the Tribological Behaviors of Carbon Fiber Reinforced Polymer Composites under Boundary Lubrication. *Polymers* **2022**, *14*, 3716. [[CrossRef](#)]
24. Xu, Z.; Lu, Z.; Zhang, J.; Li, D.; Liu, J.; Lin, C. The friction and wear behaviours of Inconel 718 superalloys at elevated temperature. *Front. Mater.* **2021**, *8*, 794701. [[CrossRef](#)]

Disclaimer/Publisher’s Note: The statements, opinions and data contained in all publications are solely those of the individual author(s) and contributor(s) and not of MDPI and/or the editor(s). MDPI and/or the editor(s) disclaim responsibility for any injury to people or property resulting from any ideas, methods, instructions or products referred to in the content.